Numerical representation of geostrophic modes on arbitrarily structured C-grids

J. Thuburn [a,*], T. D. Ringler [b] W. C. Skamarock [c]
J. B. Klemp [c]

[a] *Mathematics Research Institute, School of Engineering, Mathematics and Physical Sciences, University of Exeter, Exeter, EX4 4QF, UK*

[b] *Theoretical Division, Los Alamos National Laboratory, Los Alamos, New Mexico 87545, USA*

[c] *National Center for Atmospheric Research, Boulder, Colorado 80307, USA*

Abstract

A C-grid staggering, in which the mass variable is stored at cell centers and the normal velocity component is stored at cell faces (or edges in two dimensions) is attractive for atmospheric modeling since it enables a relatively accurate representation of fast wave modes. However, the discretization of the Coriolis terms is non-trivial. For constant Coriolis parameter, the linearized shallow water equations support geostrophic modes: stationary solutions in geostrophic balance. A naive discretization of the Coriolis terms can cause geostrophic modes to become non-stationary, causing unphysical behaviour of numerical solutions. Recent work has shown how to discretize the Coriolis terms on a planar regular hexagonal grid to ensure that geostrophic modes are stationary while the Coriolis terms remain energy conserving. In this paper this result is extended to arbitrarily structured C-grids. An explicit formula is given for constructing an appropriate discretization of the Coriolis terms. The general formula is illustrated by showing that it recovers previously known results for the planar regular hexagonal C-grid and the spherical longitude-latitude C-grid. Numerical calculation confirms that the scheme does indeed give stationary geostrophic modes for the hexagonal-pentagonal and triangular geodesic C-grids on the sphere.

* Corresponding author
Email addresses: j.thuburn@ex.ac.uk (J. Thuburn), ringler@lanl.gov (T. D. Ringler), skamaroc@ucar.edu (W. C. Skamarock), klemp@ucar.edu (J. B. Klemp).

1 Introduction

Atmospheric and oceanic flows are balance-dominated on large scales. Accurate representation of balance in numerical models requires an accurate representation of the fast acoustic and inertio-gravity waves that are the mechanism for adjustment towards balance. A C-grid, in which the mass and pressure variables are stored at cell centers and normal velocity components are stored at cell faces (or cell edges in two dimensions), allows a relatively accurate representation of the fast waves provided the Rossby radius is well resolved [1,18,9] and so is often favored by atmospheric modelers.

The drawback of the C-grid is its handling of the Coriolis terms: the Coriolis term at any face requires a value of the tangential velocity at that face, which must therefore be approximated using a suitable weighted average of normal velocity components from nearby faces. The ability of the resulting scheme to capture wave propagation accurately can be sensitive to the details of the stencil and weights used for this averaging [27,8,25,26].

The present work is motivated by the possibility of using a hexagonal-pentagonal geodesic grid with a C-grid staggering for global atmospheric modeling. Geodesic grids (both hexagonal and triangular versions, though not necessarily with C-grid staggering) were proposed in the late 1960's [28,21,7,14], and there is now renewed interest because the nearly homogeneous and isotropic grid avoids pole problems and is expected to permit good performance on massively parallel computer architectures [11,24,23,10,19,13,20,4,15,22]. However, despite the promise of such grids, initial studies of wave propagation for the linearized f-plane shallow water equations using a perfectly regular hexagonal C-grid revealed a potential problem: with the most obvious discretization of the Coriolis terms, geostrophic modes, which should have zero frequency, in fact have non-zero frequencies, with the largest being of the same order as the Coriolis parameter f [16]. Thuburn [26] and, independently, Klemp and Skamarock (unpublished report) showed how to modify the discretization of the Coriolis terms on the regular hexagonal f-plane C-grid to ensure stationary geostrophic modes. However, they left open the question of how to extend this construction to the distorted hexagons and the pentagons of the spherical geodesic grid. This extension is the topic of the present paper.

Although motivated by one particular grid, our procedure for constructing a discretization of the Coriolis terms is, in fact, applicable to a wide variety of grid structures. To define the class of permitted grids consider the *dual grid*. The vertices of the dual grid coincide with the cell centers of the orginal or *primal grid*, the dual grid cell centers correspond to primal grid vertices, and each dual edge crosses exactly one primal edge. Our procedure is applicable to grids having the property that dual edges are orthogonal to primal edges.

The allowed grids include arbitrary Delaunay triangulations and Voronoi diagrams (e.g. [3]), as well as quadrilateral grids based on orthogonal coordinate systems such as longitude-latitude and conformal cubed sphere (e.g. [17]). Unstructured versions of such grids, called *unstructured orthogonal grids*, have been applied, for example, to coastal and shelf modelling [5,6], though without explicitly addressing the issue of stationarity of geostrophic modes.

To keep clear the wide applicability of our construction of the Coriolis terms, we present it in section 2 below for the linearized constant f shallow water equations in a general framework. In section 3 we show that the proposed scheme maintains energy conservation. In section 4 we illustrate how our procedure works for several example grid structures. The derivation gives insight into previous results showing sensitivity of Rossby wave propagation to the handling of the Coriolis terms on a longitude-latitude spherical C-grid [27]. The construction presented here will also be applicable to a wide variety of other grids, including conformal cubed sphere and arbitrarily structured and adaptively refined grids.

2 Derivation of Coriolis term weighting factors

The rotating shallow water equations, linearized about a state of rest with constant mean geopotential Φ_0, may be written

$$\frac{\partial \Phi}{\partial t} + \Phi_0 \delta = 0, \tag{1}$$

$$\frac{\partial \mathbf{u}}{\partial t} + f\mathbf{k} \times \mathbf{u} + \nabla \Phi = 0. \tag{2}$$

Here $\mathbf{u}$ is the horizontal velocity vector, $\mathbf{k}$ is the unit vertical vector, f is the Coriolis parameter, ∇ is the horizontal gradient operator, and $\delta = \nabla \cdot \mathbf{u}$ is the velocity divergence. The geometry is two-dimensional, but may be planar or some curved surface such as the surface of a sphere.

In this paper we will restrict attention to the case of constant Coriolis parameter f, allowing us to focus on the requirement that geostrophic modes should be stationary. Although, for a spherical planet, variations in f are inherently associated with the spherical geometry, in fact there is no *mathematical* inconsistency in taking f to be constant in a curved geometry. We will exploit this fact in order to test our approach in section 4.

The key insight needed to motivate the derivation below comes from the linearized vorticity equation (obtained by taking $\mathbf{k} \cdot \nabla \times$ (2))

$$\frac{\partial \xi}{\partial t} + f\delta = 0, \tag{3}$$

where

$$\xi = \mathbf{k} \cdot \nabla \times \mathbf{u} \tag{4}$$

is the relative vorticity. For geostrophic modes the divergence vanishes, implying that the vorticity tendency must vanish; thus, geostrophic modes must be stationary. We wish to develop numerical schemes that have an analogue of this property that vanishing divergence implies steady vorticity. This will be achieved by ensuring that the divergence that appears in the discrete vorticity equation is consistent with the divergence that appears in the discrete mass equation.

Now consider a C-grid discretization of (1) and (2). Figure 1 shows part of a polygonal grid. The cells, vertices and edges are numbered arbitrarily; this numbering will be used to give concrete examples illustrating the general formulas derived below. The geometrical quantities needed to define a C-grid scheme and for the derivation below are shown in Fig. 2. These are l_e the length of primal edge e, d_e the length of dual edge e, A_i the area of primal cell i, and $A_v^{(\mathrm{v})}$ the area of dual cell v. (For this last quantity, the superscript label (v) indicates that the area is associated with a vertex of the primal grid, while the subscript index v indicates which vertex.) The prognostic variables are the geopotential stored at cell centers (or, better, regarded as cell averages) Φ_i, and the normal component of velocity stored at cell edges u_e (Fig. 3). In order to remove the ambiguity in the sign of u_e we define a unit normal vector $\mathbf{n}_e$ at each edge that points in the direction of positive u_e (Fig. 2). We also define an indicator function $n_{e\,i}$: when edge e is an edge of cell i $n_{e\,i} = 1$ if $\mathbf{n}_e$ is an *outward* normal of cell i and $n_{e\,i} = -1$ if $\mathbf{n}_e$ is an *inward* normal of cell i.

In the derivation that follows we will need some notation to describe the connectivity of the grid. The notation used is summarized in Table 1.

The discrete form of the mass equation is

$$\frac{\partial \Phi_i}{\partial t} + \Phi_0 \delta_i = 0, \tag{5}$$

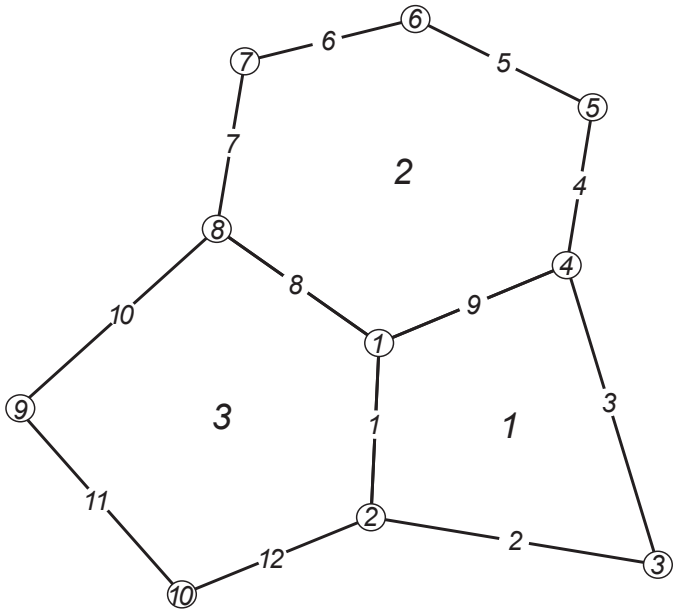

Fig. 1. Schematic showing part of an arbitrary polygonal grid. Cells, edges and vertices are each numbered with unique but otherwise arbitrary indices; this numbering will be used to give concrete examples illustrating more general formulas.

where δ_i, the discrete divergence in cell i, is defined in a natural way via the divergence theorem:

$$A_i \delta_i = \sum_{e \in \mathrm{EC}(i)} n_{e\,i} l_e u_e. \tag{6}$$

The discrete momentum equation is

$$\frac{\partial u_e}{\partial t} + f u^{\perp}{}_e - \frac{1}{d_e} \sum_{i \in \mathrm{CE}(e)} n_{e\,i} \Phi_i = 0, \tag{7}$$

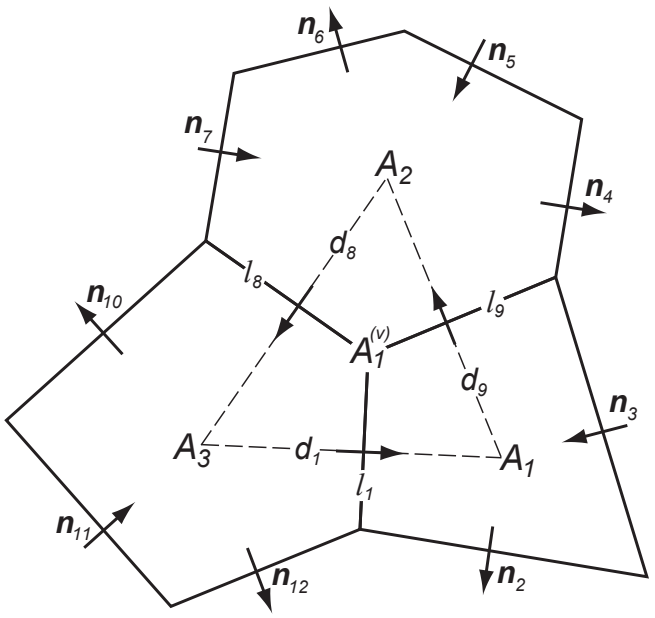

Fig. 2. Schematic showing the geometrical information needed to define a C-grid scheme on an arbitrary polygonal grid: primal edges are shown by continuous lines and dual edges by dashed lines; l_e is the length of primal edge e; d_e is the length of dual edge e; A_i is the area of primal cell i; $A_v^{(\mathrm{v})}$ is the area of dual cell v; $\mathbf{n}_e$ is the unit normal at edge e indicating the direction corresponding to positive u_e.

where the discrete gradient is given by a natural centered difference approximation. As usual on a C-grid, the awkward part of the discretization is how to approximate the Coriolis terms, since we require the velocity component ${u^\perp}_e$ in the direction $-\mathbf{k} \times \mathbf{n}_e$ orthogonal to the normal component that naturally resides at edge e.

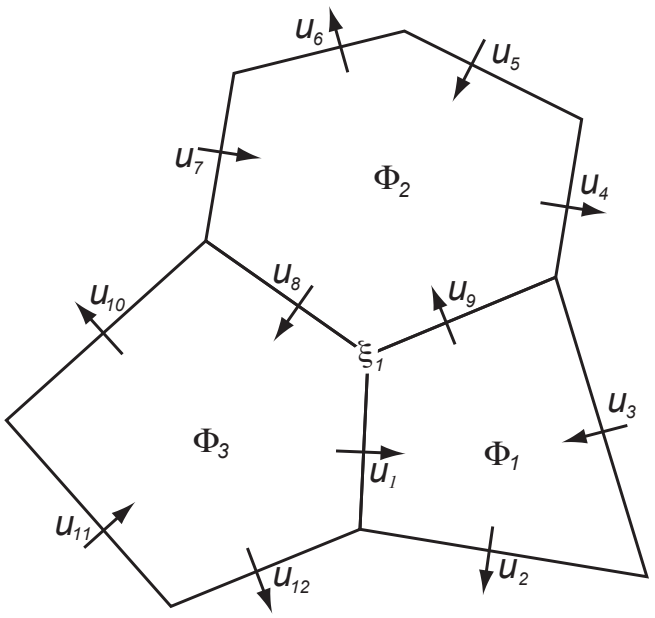

Fig. 3. Schematic showing the locations of the prognostic variables Φ_i and u_e, as well as the natural location for diagnosing the relative vorticity ξ at vertex 1.

We assume that ${u^\perp}_e$ is given by some weighted combination of the normal velocities at the edges surrounding the two cells either side of edge e:

$$d_e {u^\perp}_e = \sum_{e' \in \mathrm{ECP}(e)} w_{e\,e'} l_{e'} u_{e'}. \tag{8}$$

Inspired by Arakawa and Lamb's scheme [2] for a longitude-latitude grid, we include the length factors l_e and d_e in this formula in the expectation that this will lead to simplifications later. (We also anticipate that the extension to the full nonlinear case will work in terms of mass fluxes - Ringler et al., manuscript submitted to Journal of Computational Physics.) Our task now is

Table 1. Summary of notation used to describe the grid connectivity.

Edges of Cell i	$\mathrm{EC}(i)$
Edges incident on Vertex v	$\mathrm{EV}(v)$
Cells either side of Edge e	$\mathrm{CE}(e)$
Cells surrounding Vertex v	$\mathrm{CV}(v)$
Vertices of Cell i	$\mathrm{VC}(i)$
Vertices at the ends of Edge e	$\mathrm{VE}(e)$
Edges of a Cell Pair meeting at edge e	$\mathrm{ECP}(e) = \cup_{i \in \mathrm{CE}(e)} \mathrm{EC}(i)$
Edge pair meeting at a Vertex v of Cell i	$\mathrm{EVC}(v, i)$
Edges meeting at Vertex v that each share a cell with Edge e	$\mathrm{EVE}(v, e)$

to find suitable weights $w_{e\,e'}$ such that the Coriolis terms give no net source or sink of energy and geostrophic modes are stationary. It is physically reasonable to set $w_{e\,e} = 0$ for all e, so that u_e does not contribute to ${u^\perp}_e$. The requirement that the Coriolis terms be energy conserving also implies $w_{e\,e} = 0$ (see (39) below). We therefore build in this assumption from the start. For the grid shown in Figs. 1-3, for example, ${u^\perp}_1$ is given by a weighted combination of u_2, u_3, u_9, u_8, u_{10}, u_{11}, and u_{12}.

Now seek a discrete analogue of the vorticity equation. On a C-grid the relative vorticity ξ_v is naturally defined at vertices via Stokes' theorem applied to a dual cell:

$$A_v^{(\mathrm{v})} \xi_v = \sum_{e \in \mathrm{EV}(v)} d_e u_e t_{e\,v}. \tag{9}$$

Here we have introduced another indicator function $t_{e\,v}$, which is equal to 1 when vertex v is at the left end of edge e (i.e. in the direction $\mathbf{k} \times \mathbf{n}_e$) and equal to -1 if vertex v is at the right end of edge e. This indicator function ensures that counterclockwise circulation about vertex v contributes positively to the vorticity at vertex v. For the grid shown in Figs. 1-3, for example, $t_{1\,1}$, $t_{9\,1}$ and $t_{8\,1}$ would all equal 1 because u_1, u_9 and u_8 all contribute positively to the circulation about vertex 1. This definition of ξ_v depends on the orthogonality of primal and dual edges, since it requires the normal velocity at a primal edge to equal the tangential velocity at the corresponding dual edge.

Using the definitions (9) and (8) and the discrete momentum equation (7), the vorticity tendency is given by

$$
\begin{aligned}
A_v^{(\mathrm{v})}\frac{\partial \xi_v}{\partial t} &= \sum_{e\in \mathrm{EV}(v)} d_e \frac{\partial u_e}{\partial t} t_{e\,v} \\
&= -\sum_{e\in \mathrm{EV}(v)} f d_e u^{\perp}{}_e t_{e\,v} + \sum_{e\in EV(v)} t_{e\,v} \sum_{i\in \mathrm{CE}(e)} n_{e\,i}\Phi_i \\
&= -f \sum_{e\in \mathrm{EV}(v)} \sum_{e'\in \mathrm{ECP}(e)} w_{e\,e'} l_{e'} u_{e'} t_{e\,v}. \qquad (10)
\end{aligned}
$$

(It may be verified that each Φ_i that appears does so twice, once with a plus sign and once with a minus sign. Thus all contributions involving Φ cancel, giving a discrete analog of the identity $\nabla \times \nabla\Phi \equiv 0$.) If we demand that a discrete analogue of (3) should hold then the right hand side of (10) should equal

$$
-f A_v^{(\mathrm{v})} \delta_v^{(\mathrm{v})} \qquad (11)
$$

for some discrete analogue of the divergence $\delta_v^{(\mathrm{v})}$ at vertex v.

In order for geostrophic modes to be stationary the vertex divergence $\delta_v^{(\mathrm{v})}$ must vanish whenever the cell divergence δ_i vanishes for all cells i. A natural way to impose this requirement is to demand that $\delta_v^{(\mathrm{v})}$ be given by a remapping of δ_i:

$$
A_v^{(\mathrm{v})}\delta_v^{(\mathrm{v})} = \sum_{i\in \mathrm{CV}(v)} R_{i\,v} A_i \delta_i \qquad (12)
$$

for some weights $R_{i\,v}$. These weights may be thought of as residing at cell corners (Fig. 4). We have some freedom in the choice of weights, but they must satisfy

$$
\sum_{v\in \mathrm{VC}(i)} R_{i\,v} = 1 \qquad (13)
$$

in order to preserve the global integral of divergence: $\sum_v A_v^{(\mathrm{v})}\delta_v^{(\mathrm{v})} = \sum_i A_i \delta_i$.

Substituting (6) in (12) and combining with (10) and (11) gives

$$
\sum_{i\in \mathrm{CV}(v)} R_{i\,v} \sum_{e\in \mathrm{EC}(i)} n_{e\,i} l_e u_e = \sum_{e\in \mathrm{EV}(v)} \sum_{e'\in \mathrm{ECP}(e)} w_{e\,e'} l_{e'} u_{e'} t_{e\,v}. \qquad (14)
$$

We require this to hold for arbitrary values of the cell-edge normal velocities. First consider an edge e' and a vertex v of cell i such that vertex v *is not* at one end of edge e', (for example, edge $e' = 1$ and vertex $v = 8$ of cell $i = 3$ in

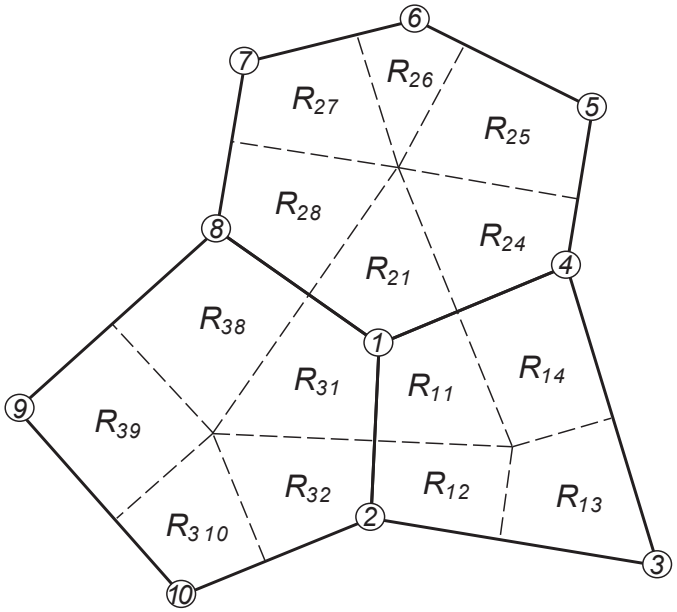

Fig. 4. Schematic showing the locations of the weights $R_{i\,v}$ that define the vertex divergence in terms of the cell divergence.

Figs. 1-4). The contribution to the left hand side of (14) involving velocity $u_{e'}$ is

$$R_{i\,v} n_{e'\,i} l_{e'} u_{e'}, \tag{15}$$

while the contribution to the right hand side is

$$\sum_{e \in EVC(v,i)} w_{e\,e'} l_{e'} u_{e'} t_{e\,v}. \tag{16}$$

(In our example EVC$(8,3)$ is the edge pair $\{8,10\}$. Edge 1 contributes to the vorticity tendency at vertex 8 through its contribution to ${u^\perp}_8$ and ${u^\perp}_{10}$, while it contributes to the divergence at vertex 8 through $R_{3\,8}$ times its contribution to the divergence in cell 3.) Equating the contributions (15) and (16) gives

$$\sum_{e \in \mathrm{EVC}(v,i)} w_{e\,e'} t_{e\,v} = R_{i\,v} n_{e'\,i}. \tag{17}$$

Now consider an edge e' and a vertex v that *is* at one end of edge e', (for example, edge $e' = 1$ and vertex $v = 1$ in Figs. 1-4). The contribution to the left hand side of (14) involving velocity $u_{e'}$ is

$$\sum_{i \in \mathrm{CE}(e')} R_{i\,v} n_{e'\,i} l_{e'} u_{e'}, \tag{18}$$

while the contribution to the right hand side is

$$\sum_{e \in \mathrm{EVE}(v,e')} w_{e\,e'} l_{e'} u_{e'} t_{e\,v}. \tag{19}$$

(In our example EVE$(1,1)$ is the edge pair $\{8,9\}$. Edge 1 contributes to the vorticity tendency at vertex 1 through its contribution to ${u^\perp}_8$ and ${u^\perp}_9$ while it contributes to the divergence at vertex 1 through $R_{3\,1}$ times its contribution to the divergence in cell 3 and $R_{1\,1}$ times its contribution to the divergence in cell 1.) Equating the contributions (18) and (19) gives

$$\sum_{e \in \mathrm{EVE}(v,e')} w_{e\,e'} t_{e\,v} = \sum_{i \in \mathrm{CE}(e')} R_{i\,v} n_{e'\,i}. \tag{20}$$

For any given e', the equations (17) and (20) constitute a system of linear simultaneous equations for the weights $w_{e\,e'}$ given the $R_{i\,v}$. The linear system contains a single equation for each vertex v associated with the cells on either side of edge e'. In our example, the edge $e' = 1$ gives rise to 7 equations for 7 unknowns:

$$\begin{aligned}
w_{8\,1} + w_{9\,1} &= -R_{1\,1} + R_{3\,1},\\
-w_{10\,1} - w_{8\,1} &= R_{3\,8},\\
w_{11\,1} + w_{10\,1} &= R_{3\,9},\\
-w_{12\,1} - w_{11\,1} &= R_{3\,10},\\
-w_{2\,1} + w_{12\,1} &= R_{3\,2} - R_{1\,2},\\
w_{3\,1} + w_{2\,1} &= -R_{1\,3},\\
-w_{9\,1} - w_{3\,1} &= -R_{1\,4}.
\end{aligned} \tag{21}$$

For the general case, let us write the linear system compactly as

$$\mathbf{A}\mathbf{w} = \mathbf{R}, \tag{22}$$

where $\mathbf{w}$ is the vector of unknown weights, $\mathbf{R}$ is the vector of right hand sides, and $\mathbf{A}$ is the coefficient matrix. In fact this system of equations is singular. If we add together all the equations in the system for a given e' we find that each $w_{e\,e'}$ appears exactly twice, once with $t_{e\,v} = 1$ and once with $t_{e\,v} = -1$ so that the total left hand side vanishes, i.e.

$$\mathbf{c}^T\mathbf{A} = \mathbf{0}, \tag{23}$$

where $\mathbf{c}$ is a column vector whose elements are all equal to 1. Therefore, the system can have a solution only if a certain solvability condition is satisfied. The solvability condition is obtained by taking $\mathbf{c}^T$ times (22), implying $\mathbf{c}^T\mathbf{R} = 0$, in other words the sum of all the right hand sides should also equal zero:

$$\sum_{i\in\mathrm{CE}(e')} \sum_{v\in\mathrm{VC}(i)} R_{i\,v} n_{e'\,i} = 0. \tag{24}$$

Using (13), this reduces to

$$\sum_{i\in\mathrm{CE}(e')} n_{e'\,i} = 0, \tag{25}$$

which is indeed satisfied. The singular nature of the linear system, and the fact that the solvability condition is satisfied, are easily verified for the example (21) by adding the component equations.

Because the solvability condition is satisfied, the linear system not only has a solution, but has a non-unique solution; because $\mathbf{A}$ is singular there exists a $\tilde{\mathbf{w}}$ satisfying $\mathbf{A}\tilde{\mathbf{w}} = 0$, and we may add any multiple of $\tilde{\mathbf{w}}$ to a solution $\mathbf{w}$ of (22) to obtain another solution.

This non-uniqueness means we have the freedom to introduce one further constraint into each system of linear equations. We will choose a constraint that causes the system of linear equations for a given e' to split into two independent subsystems, with the property that each subsystem involves w's and R's from only one of the cells either side of edge e'. This splitting is essential to allow an energy conserving scheme to be found. To split the system, replace (20) by two equations of the form

$$w_{e\,e'} t_{e\,v} = (R_{i\,v} - \alpha_{e'\,i\,v})\, n_{e'\,i}, \tag{26}$$

one equation for each cell i either side of edge e'. In each case the relevant e is defined by the fact that e' and e are edges of cell i that meet at vertex v. The $\alpha_{e'\,i\,v}$ are some constants that are to be determined, subject to some constraints discussed below; for each linear system four α's appear, two in each subsystem. For example, the system (21) splits into the two subsystems

$$\begin{aligned} w_{8\,1} &= R_{3\,1} + \alpha_{1\,1\,3}, \\ -w_{10\,1} - w_{8\,1} &= R_{3\,8}, \\ w_{11\,1} + w_{10\,1} &= R_{3\,9}, \\ -w_{12\,1} - w_{11\,1} &= R_{3\,10}, \\ w_{12\,1} &= R_{3\,2} - \alpha_{1\,2\,3}, \end{aligned} \tag{27}$$

involving edges and R's only from cell 3, and

$$\begin{aligned} -w_{2\,1} &= -R_{1\,2} + \alpha_{1\,2\,1}, \\ w_{3\,1} + w_{2\,1} &= -R_{1\,3}, \\ -w_{9\,1} - w_{3\,1} &= -R_{1\,4}, \\ w_{9\,1} &= -R_{1\,1} - \alpha_{1\,1\,1}, \end{aligned} \tag{28}$$

involving edges and R's only from cell 1.

In order to recover (20) from the components into which it has been split, we require

$$\sum_{i \in \mathrm{CE}(e')} \alpha_{e'\,i\,v} n_{e'\,i} = 0 \tag{29}$$

for each e' and $v \in \mathrm{VE}(e')$.

Now we have one more equation than unknown in each subsystem: one equation for each vertex v of cell i, and one unknown $w_{e\,e'}$ for each edge e of cell i except for $e = e'$. Thus each subsystem will have a solution only if it satisfies its own solvability condition. Again, the solvability condition is obtained by summing the individual equations in the subsystem to obtain

$$\sum_{v \in \mathrm{VC}(i)} R_{i\,v} - \sum_{v \in \mathrm{VE}(e')} \alpha_{e'\,i\,v} = 0. \tag{30}$$

Using (13), this reduces to

$$\sum_{v \in \mathrm{VE}(e')} \alpha_{e'\,i\,v} = 1. \tag{31}$$

Thus, the four α values associated with edge e' must be related to each other by (29) and (31). The simplest choice that satisfies these constraints is to set

$$\alpha_{e'\,i\,v} = 1/2 \tag{32}$$

for all e', $i \in \mathrm{CE}(e')$ and $v \in \mathrm{VE}(e')$. We will show in section 3 that this choice also makes the scheme energy conserving, and, moreover, is the only such choice. This choice will be used in the examples discussed in section 4.

For each edge e', equations (17) and (26) now form a closed linear subsystem for the $w_{e\,e'}$ with $e \in \mathrm{EC}(i)$ that has a unique solution. In fact the solution for $w_{e\,e'}$ may be found explicitly by summing (17) and (26) over the vertices between edge e' and edge e:

$$\begin{aligned} w_{e\,e'} t_{e\,v_2} &= \left(\sum_v R_{i\,v} - \alpha_{e'\,i\,v_1} \right) n_{e'\,i} \\ &= \left(\sum_v R_{i\,v} - 1/2 \right) n_{e'\,i}, \end{aligned} \tag{33}$$

where the vertex v_1 is the first vertex encountered in traversing from edge e' to edge e, v_2 is the last vertex encountered, and, in the second line, the α's have been set to $1/2$. The sum may be taken either clockwise or counterclockwise around cell i; the solvability condition (30) ensures that the same answer is obtained either way. For example, for the grid shown in Figs. 1-4, if we evaluate $w_{7\,4}$ by summing counterclockwise around cell 2 we would take $v_1 = 5$ and $v_2 = 7$ to obtain

$$w_{7\,4} = R_{2\,5} + R_{2\,6} + R_{2\,7} - 1/2. \tag{34}$$

3 Energy conservation

For the continuous equations (2) the Coriolis force does no work and therefore makes no net contribution to the energy budget. It is highly desirable that a numerical scheme should have an analogous property.

We may form a discrete kinetic energy equation for the linearized system by taking $A_e^{(\mathrm{e})} u_e$ times (7) and summing over edges. Here, the superscript (e) indicates that the area $A_e^{(\mathrm{e})}$ is associated with an edge, while the subscript index e identifies which edge (Fig. 5). The contribution from the Coriolis terms will vanish provided

$$\sum_e A_e^{(\mathrm{e})} u_e u^{\perp}{}_e = 0, \tag{35}$$

i.e. provided

$$\sum_e \frac{A_e^{(\mathrm{e})} u_e}{d_e} \sum_{e' \in \mathrm{ECP}(e)} w_{e\,e'} l_{e'} u_{e'} = 0, \tag{36}$$

where the sums over e are over all edges on the grid.

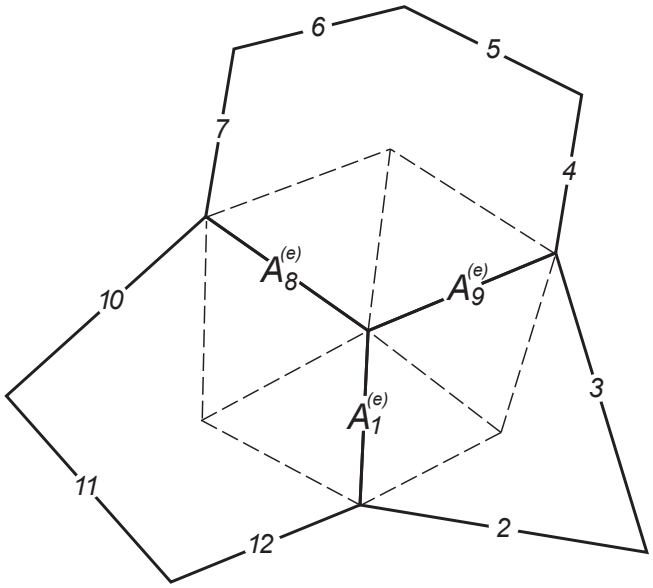

Fig. 5. Schematic showing the areas $A_1^{(\mathrm{e})}$, $A_9^{(\mathrm{e})}$, and $A_8^{(\mathrm{e})}$ associated with edges 1, 9, and 8. The area associated with edge 1 comprises the two triangles either side of edge 1.

The contribution involving $u_e u_{e'}$ will vanish provided

$$\frac{A_e^{(\mathrm{e})} l_{e'}}{d_e} w_{e\,e'} + \frac{A_{e'}^{(\mathrm{e})} l_e}{d_{e'}} w_{e'\,e} = 0, \tag{37}$$

i.e. provided

$$\frac{l_{e'}d_{e'}}{A^{(\mathrm{e})}_{e'}}w_{e\,e'} + \frac{l_e d_e}{A^{(\mathrm{e})}_{e}}w_{e'\,e} = 0. \tag{38}$$

In planar geometry the orthogonality of primal and dual edges implies $A^{(\mathrm{e})}_e = l_e d_e/2$. In curved geometry we can used this relation to define $A^{(\mathrm{e})}_e$, making a very good approximation to the actual kite-shaped area associated with edge e. [1] Assuming this choice, energy conservation by the Coriolis terms then requires

$$w_{e\,e'} + w_{e'\,e} = 0. \tag{39}$$

Using the explicit expression (33) for the weights derived in section 2, we find

$$w_{e\,e'} + w_{e'\,e} = \left(\sum_v R_{i\,v} - \alpha_{e'\,i\,v_1}\right) n_{e'\,i} t_{e\,v_2} + \left(\sum_v R_{i\,v} - \alpha_{e\,i\,v_2}\right) n_{e\,i} t_{e'\,v_1}. \tag{40}$$

It may easily be verified that $n_{e'\,i}t_{e\,v_2} + n_{e\,i}t_{e'\,v_1}$ must always vanish. Therefore the Coriolis terms will be energy conserving provided

$$\alpha_{e'\,i\,v_1} = \alpha_{e\,i\,v_2}. \tag{41}$$

The choice $\alpha_{e\,i\,v} = 1/2$ for all e, i and v, certainly satisfies this constraint as well as the constraints (29) and (31) of section 2.

In fact it can be shown that for any grid $\alpha_{e\,i\,v} = 1/2$ for all e, i and v is the only such choice. Application of the constraint (41) for different edges and vertices of any cell i leads to the conclusion that all α's associated with cell i must take the same value. The constraint (31) then implies that that value must equal 1/2.

[1] Derivation of the full energy budget shows that the global kinetic energy must be defined as $\sum_e l_e d_e \Phi_0 u_e^2/2$. This may be interpreted in various ways. One can regard $\Phi_0 u_e^2/2$ as the kinetic energy density associated with an area $A^{(\mathrm{e})}_e = l_e d_e$ twice that suggested in the text. Alternatively, one can regard $\Phi_0 u_e^2/2$ as *half* the kinetic energy density (since it includes only the normal velocity component and not the tangetial component) associated with an area $A^{(\mathrm{e})}_e = l_e d_e/2$.

4 Examples

4.1 Planar square grid

The simplest possible C-grid comprises a grid of square cells on a plane. Let the cell width be d, so that $l_e = d$ and $d_e = d$ for all edges e. The simplest and most symmetrical choice is to set $R_{i\,v} = 1/4$ for the four vertices v of each cell i, so that each cell contributes one quarter of its divergence to each of its four vertices. To be concrete, consider the cell, edge and vertex numbering shown in Fig. 6. Taking $e' = 1$, formula (33) gives

$$\begin{aligned} -w_{2\,1} &= R_{1\,1} - 1/2 = -1/4, \\ w_{3\,1} &= R_{1\,1} + R_{1\,2} - 1/2 = 0, \\ w_{4\,1} &= R_{1\,1} + R_{1\,2} + R_{1\,4} - 1/2 = 1/4, \end{aligned} \tag{42}$$

for the contributions of u_1 to ${u^\perp}_2$, ${u^\perp}_3$, and ${u^\perp}_4$, with similar expressions for the other weights relating the edges of cell 1. In terms of the more familiar notation where u signifies the eastward velocity component and v the northward component, we obtain the most obvious discretization, in which v at a u point is given by the average (with weights 1/4) of the nearest four v values and u at a v point is given by the average of the nearest four u values. It is well known that the f-plane dispersion relation for this discretization does have $\omega = 0$ as a root, confirming that its geostrophic modes are indeed stationary.

As an aside, we note that a higher order discretization of the Coriolis terms has been proposed by Dobricic [8]. Although the Dobricic scheme does not fit within the framework permitted by our analysis, because it uses a larger stencil, it does give stationary geostrophic modes on a square planar grid. However, as is evident from [27] and example 4.3 below, care will be needed when extending that scheme to a longitude-latitude grid in spherical geometry.

4.2 Planar regular hexagonal grid

Now consider a perfectly regular hexagonal C-grid in planar geometry, with numbering as in Fig. 7. Let the distance between neighboring cell centers be d, so that $l_e = d/\sqrt{3}$ and $d_e = d$ for every edge e. The simplest and most symmetrical choice is to set $R_{i\,v} = 1/6$ for the six vertices v of every cell i, so that each cell shares its divergence equally among its six vertices. Using the numbering in Fig. 7, equation (33) then gives

$$w_{2\,1} = R_{1\,1} - 1/2 = -1/3,$$

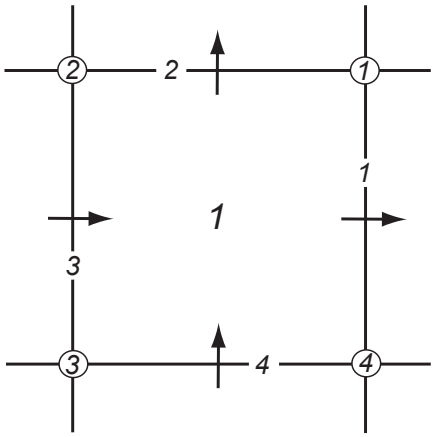

Fig. 6. Schematic showing the cell, edge and vertex numbering, and unit normal vectors at cell edges, for part of a square grid.

$$\begin{aligned} -w_{3\,1} &= R_{1\,1} + R_{1\,2} - 1/2 = -1/6, \\ w_{4\,1} &= R_{1\,1} + R_{1\,2} + R_{1\,4} - 1/2 = 0, \\ -w_{5\,1} &= R_{1\,1} + R_{1\,2} + R_{1\,4} + R_{1\,5} - 1/2 = 1/6, \\ w_{6\,1} &= R_{1\,1} + R_{1\,2} + R_{1\,4} + R_{1\,5} + R_{1\,6} - 1/2 = 1/3, \end{aligned} \tag{43}$$

for the contributions of u_1 to ${u^\perp}_2$, ${u^\perp}_3$, ${u^\perp}_4$, ${u^\perp}_5$, and ${u^\perp}_6$, with similar expressions for the other weights relating the edges of cell 1. Taking into account the weighting by d_e and $l_{e'}$ in (8), it may be verified that these weights agree with those given by [26] and by Klemp and Skamarock (unpublished report). Those authors confirmed that these weights do indeed give stationary geostrophic modes on the f-plane.

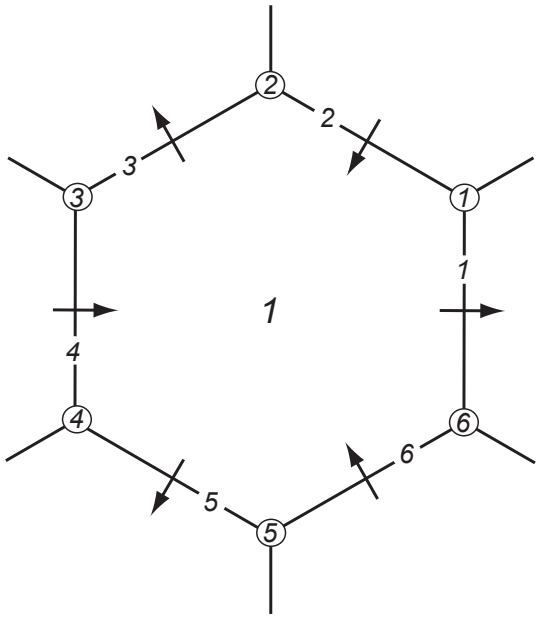

Fig. 7. Schematic showing the cell, edge and vertex numbering, and unit normal vectors at cell edges, for part of a regular hexagonal grid.

4.3 Longitude-latitude grid on the f-sphere

The derivation presented here is motivated by the need for discretizations in spherical geometry. However, allowing f to vary with latitude would provide a propagation mechanism for Rossby waves, obscuring the issue of whether the slow modes are accurately represented. We therefore introduce the idea of the "f-sphere": the geometry is spherical, but the Coriolis parameter is set to a constant. This allows us to capture the effects of the spherical geometry on the grid structure, but within a system that still supports stationary geostrophic modes, as we show next.

To find the dispersion relation for the continuous linearized shallow water equations on the f-sphere, first form the vorticity and divergence equations by taking $\mathbf{k} \cdot \nabla\times(2)$ and $\nabla\cdot(2)$:

$$\frac{\partial \xi}{\partial t} + f\delta = 0, \tag{44}$$

$$\frac{\partial \delta}{\partial t} - f\xi + \nabla^2\Phi = 0. \tag{45}$$

Now eliminate ξ and δ using the mass continuity equation (1) to obtain

$$\frac{\partial^3 \Phi}{\partial t^3} + f^2\frac{\partial \Phi}{\partial t} - \Phi_0\nabla^2\frac{\partial \Phi}{\partial t} = 0. \tag{46}$$

This equation supports normal mode solutions with Φ proportional to the spherical harmonic $Y_m^n(\lambda, \sin\phi)$, where λ is longitude and ϕ is latitude, with frequency ω satisfying the dispersion relation

$$\omega\left\{\omega^2 - f^2 - n(n+1)\Phi_0/a^2\right\} = 0, \tag{47}$$

where a is the Earth's radius. Here n must be a natural number. For $n = 0$ only the $\omega = 0$ root is physically realizable, corresponding to the trivial geostrophic mode $\Phi = \text{const}$, $\xi = \delta = 0$. For $n > 0$ there are linearly independent spherical harmonics for integer $m \in \{-n, ..., 0, ..., n\}$, and for each such m all three roots of (47) are realizable; the $\omega = 0$ root corresponds to a geostrophic mode and the non-zero roots to inertio-gravity modes.

Now consider a C-grid discretization on a longitude-latitude grid with uniform longitude spacing $\Delta\lambda$ and uniform latitude spacing $\Delta\phi$. The lengths of the eastern and western cell edges and the distances between centers of neighboring cells at the same longitude are all equal to $a\Delta\phi$. The lengths of the northern and southern cell edges and the distances between centres of neighboring cells at the same latitude are proportional to the cosine of the relevant latitude. If we assume that the non-zero $R_{i\,v}$ are all equal to $1/4$, as on the planar square grid, then (33) leads to the following discretization of the component momentum equations:

$$\frac{\partial u}{\partial t} - f\overline{\frac{1}{\cos\phi}\overline{v\cos\phi}^{\phi}}^{\lambda} + \frac{1}{a\cos\phi}\delta_\lambda\Phi = 0, \tag{48}$$

$$\frac{\partial v}{\partial t} + f\overline{\overline{u}^{\lambda}}^{\phi} + \frac{1}{a}\delta_\phi\Phi = 0. \tag{49}$$

Here, u and v are the usual eastward and northward velocity components, δ_λ and δ_ϕ are the C-grid centered difference approximations to $\partial/\partial\lambda$ and $\partial/\partial\phi$,

and an overline indicates an equally-weighted two-point average, with the superscript indicating the spatial direction of the average. Note how the $\cos\phi$ terms appear within the averages involved in the fv term.

Direct numerical calculation of the normal modes for this scheme, following the method of [27] but with f constant, confirms that the geostrophic modes are stationary. Interestingly, the more naive discretization that omits the $\cos\phi$ factors from the average of v is also found to support stationary geostrophic modes. However, as [27] showed, when f takes its usual north-south variation proportional to $\sin\phi$, inclusion of the $\cos\phi$ factors leads to good behavior of the entire Rossby mode spectrum, whereas omission of the $\cos\phi$ factors causes many Rossby modes to be badly misrepresented in terms of frequency and structure.

This result shows the importance of consistency of the mass and vorticity budgets, and hence the relevance of our derivation, even for non-constant f. It also shows that accurate representation of the Coriolis terms is non-trivial, and can have major consequences, even for what would appear to be the most straightforward case of a quadrilateral grid based on an orthogonal coordinate system. Thus, our derivation is also relevant to the Yin-Yang grid (e.g. [12]) and the conformal cubed sphere grid (e.g. [17]), among others.

4.4 Hexagonal-pentagonal geodesic grid on the f-sphere

On the hexagonal-pentagonal geodesic grid, the primal and dual edge lengths vary from edge to edge and so (33) does not reduce to any simpler formula. The weights $w_{e\,e'}$ must be calculated for each edge pair; they may either be tabulated or recalculated when needed.

To confirm the behaviour of the proposed scheme, we directly calculated the normal modes of the discretized shallow water equations on a hexagonal-pentagonal geodesic grid on the f-sphere. The grid comprised 642 cells and 1920 edges, giving 2562 degrees of freedom in total, with an average distance between cell centers of about 9.6×10^5 m. The Coriolis terms were evaluated using (8) and (33). Earth's radius was taken to be $a = 6371220$ m, the Coriolis parameter was set to $f = 1.4584 \times 10^{-4}\,\mathrm{s}^{-1}$, and the mean depth was taken to be 10^5 m, giving a Rossby radius of 2.1683×10^6 m.

Of the 2562 normal modes found, 1280 are geostrophic modes and 1282 are inertio-gravity modes. These numbers are consistent with a slightly modified version of the argument given by [26], who claimed that the number of geostrophic modes should equal the number of vorticity degrees of freedom while the number of inertio-gravity modes should equal the number of mass plus divergence degrees of freedom. Vorticity is naturally evaluated at vertices,

and the grid used has 1280 vertices. However, the global integral of vorticity is constrained to vanish, so in fact there are only 1279 vorticity degrees of freedom. Mass and divergence naturally reside in cells, but the global integral of divergence is constrained to vanish, so there are in fact 1283 mass plus divergence degrees of freedom. However, one of the mass degrees of freedom, $\Phi = \text{const}$, corresponds to the $n = 0$ mode, which has $\omega = 0$ and so is classed as a geostrophic mode rather than an inertio-gravity mode. Hence there should be 1280 geostrophic modes and 1282 inertio-gravity modes, as found.

Figure 8 shows the normal mode frequencies, sorted into geostrophic and inertio-gravity modes, and into ascending order within each of these categories. A similar number of frequencies given by (47) are also shown. Two points are noteworthy. First, all of the frequencies are real, implying that the scheme is stable; this is a consequence of energy conservation. Second, the geostrophic mode branch has frequencies exactly zero, as intended. The numerical inertio-gravity mode frequencies somewhat underestimate the exact frequencies for the fastest, smallest-scale modes, for which the finite-difference approximations to the gradient and divergence become less accurate. This is consistent with the results of [26]; although not perfect, the inertio-gravity wave dispersion is far superior to that on an unstaggered grid.

For comparison, Fig. 9 shows the normal mode frequencies for an alternative scheme: only the four edges that meet edge e are used to approximate ${u^\perp}_e$; this scheme reduces to the scheme analysed by [16] on a plane regular hexagonal grid. Again, all the frequencies are real. However, the geostrophic modes have non-zero frequencies, with the largest being of a size comparable to f.

4.5 Triangular geodesic grid on the f-sphere

There is current research interest in the possible use of the version of the geodesic C-grid that uses triangular primal cells; it is therefore worth confirming the behavior of the proposed scheme for this grid too. The calculation of section 4.4 was repeated for the triangular version of the grid. The grid now comprised 1280 triangular cells and 1920 edges, giving 3200 degrees of freedom in total, with an average distance between cell centers of about 5.6×10^5 m. Again, the Coriolis terms were evaluated using (8) and (33). The other problem parameters were the same as in section 4.4.

Of the 3200 normal modes found, 642 are geostrophic modes and 2558 are inertio-gravity modes, consistent with the numbers of vorticity, mass and divergence degrees of freedom on this grid. Figure 10 shows the normal mode frequencies, and confirms that the geostrophic mode frequencies are exactly zero, as intended. For comparison, Fig. 11 shows the results of a similar cal-

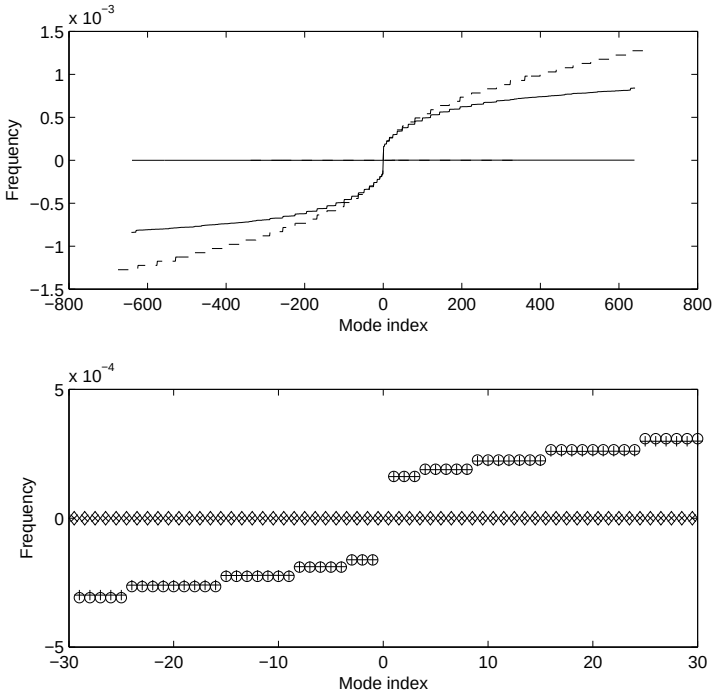

Fig. 8. Normal mode frequencies on the f-sphere. The upper panel shows the full spectrum of frequencies resolved on a hexagonal geodesic grid with 2562 degrees of freedom using the proposed scheme to compute the Coriolis terms (continuous curves) along with the exact normal mode frequencies given by (47) for $n \leq 25$ (dashed curves). The lower panel shows a subset of frequencies with smallest indices: circles and diamonds indicate exact normal mode frequencies; plus and cross symbols indicate numerical normal mode frequencies.

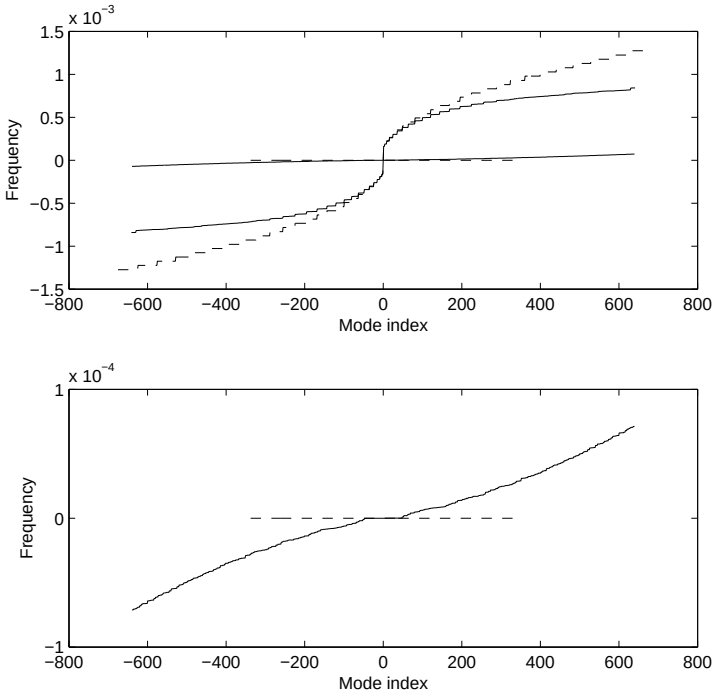

Fig. 9. Normal mode frequencies on the f-sphere. The upper panel is like the upper panel in Fig. 8 but for a scheme that reduces to the scheme used by [16] on a plane regular hexagonal grid. The lower panel shows the same data but with a much expanded frequency scale to make clear the non-zero frequencies of the geostrophic modes.

culation using a different but plausible method of constructing the tangential velocity components based on computing the angles between adjacent edges and projecting the normal velocity component at a given edge onto the tan-

gential direction of each neighboring edge. The accuracy of the inertio-gravity wave frequencies is comparable to that seen in Fig. 10, but the geostrophic mode frequencies are not exactly zero.

4.6 Computational modes

An important issue for atmosphere and ocean models, particularly in the balance-dominated flow regime, is whether the numerical solution method supports *computational modes* that fail to propagate or that propagate in an unphysical way. An advantage of the C-grid is that it does not support wave modes that spuriously fail to propagate; this result is well known for grids of orthogonal quadrilaterals (e.g. [2,18]), has been shown theoretically for regular hexagons on the plane [26], and is confirmed numerically for hexagonal and triangular geodesic grids by experiments like those described above but where f is allowed to vary with latitude.

Nevertheless, the C-grid may support wave modes that propagate in an unphysical way. The numbers and types of such modes depend on the grid structure, and are related to the numbers of vorticity, mass, and divergence degrees of freedom on the grid, as discussed above. [2]

A hexagonal C-grid, for example, has roughly twice as many Rossby modes as might be expected for a given resolution. For the case of regular hexagons on a plane, which can be analysed theoretically [26], the shallow water dispersion relation is found to be a quartic expression in frequency, with two branches corresponding to Rossby modes (rather than one branch of a cubic dispersion relation, as in the continuous case). For constant f, provided the tangential velocity appearing in the Coriolis terms is correctly constructed, the Rossby modes in the extra branch are stationary, as they should be. However, when f varies with latitude the extra Rossby modes propagate unphysically: their frequency is extremely small and of the wrong sign, and is strongly sensitive to the details of the discretization [26]. The extra Rossby modes are visible in Figs 8 and 9, though in these numerical calculations there is no simple way to distinguish which of the two branches a given mode belongs to.

A triangular C-grid, on the other hand, has roughly twice as many inertio-gravity modes as might be expected for a given resolution. For equilateral triangles on a plane the dispersion relation is a quintic in frequency, with four

[2] Incidentally, exactly the same discussion would apply to a "C-grid" vorticity-divergence formulation, in which the prognostic variables are mass and divergence in primal cells and vorticity in dual cells. This formulation would be equivalent, through (6) and (9), to the standard velocity C-grid formulation discussed in this paper.

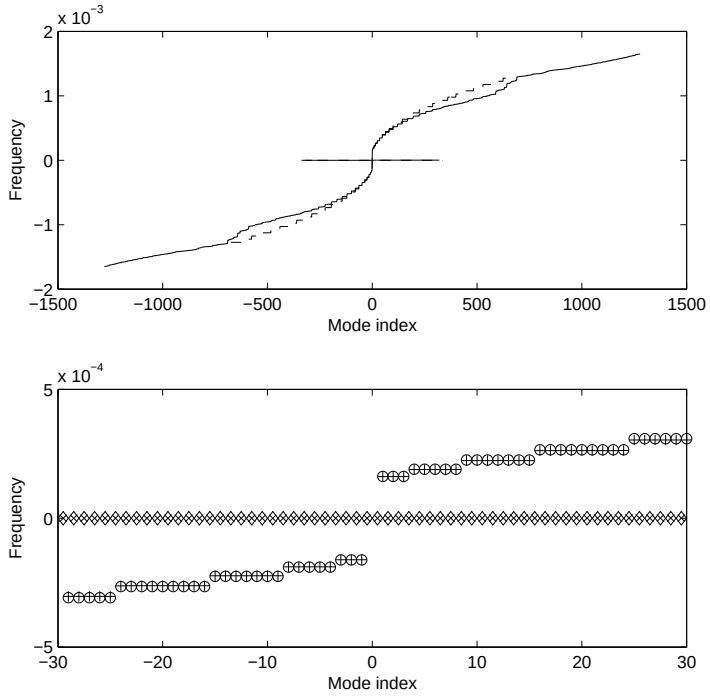

Fig. 10. Normal mode frequencies on the f-sphere. The upper panel shows the full spectrum of frequencies resolved on a triangular geodesic grid with 3200 degrees of freedom using the proposed scheme to compute the Coriolis terms (continuous curves) along with the exact normal mode frequencies given by (47) for $n \leq 25$ (dashed curves). The lower panel shows a subset of frequencies with smallest indices: circles and diamonds indicate exact normal mode frequencies; plus and cross symbols indicate numerical normal mode frequencies.

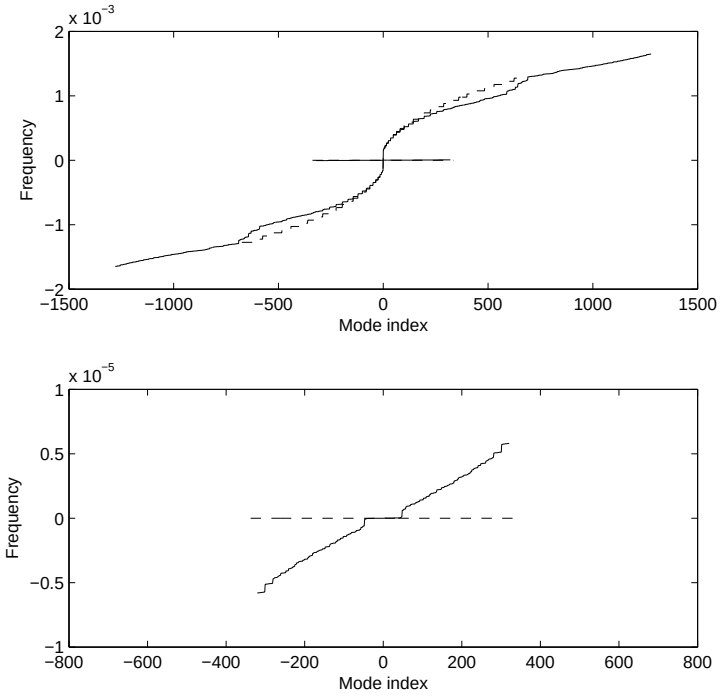

Fig. 11. Normal mode frequencies on the f-sphere. The upper panel is like the upper panel in Fig. 10 but for a scheme that constructs edge tangential velocities by projection of nearby normal velocities. The lower panel shows the same data but with a much expanded frequency scale to make clear the non-zero frequencies of the geostrophic modes.

branches corresponding to inertio-gravity modes (rather than two branches of a cubic in the continuous case). These extra inertio-gravity modes are visible in Figs 10 and 11. There is a distinct change in slope of the numerical dispersion

relation around mode index ±640 at the transition between the inertio-gravity mode branches.

The question here, then, is what effect, if any, does the construction (8) and (33) have on the presence of computational modes. The construction does not change the numbers of modes of different types; in particular, it does not introduce any new computational modes or affect the presence or otherwise of extra branches to the dispersion relation. The construction is also found to have negligible effect on inertio-gravity mode frequencies (see Figs 8 to 11 and also [26]). In the constant f case the construction has a clear benefit of eliminating spuriously fast propagation of Rossby modes (and this applies to both branches on the hexagonal and hexagonal-geodesic grids). However, in the variable f case, it does not eliminate the unphysical slow, backward propagation of the extra Rossby mode branch on the hexagonal and hexagonal-geodesic grids.

5 Discussion and conclusions

We have shown how to construct a discretization of the Coriolis terms for the linearized shallow water equations on C-grids with a wide variety of possible grid structures so as to ensure that geostrophic modes are stationary in the case of constant Coriolis parameter f. Stationarity of geostrophic modes for constant f is a pre-requisite for good Rossby mode behaviour when f varies. The proposed scheme also ensures that the Coriolis terms introduce no spurious source or sink of energy.

The tangential velocity at a cell edge is expressed as a weighted sum of the known normal velocities at a set of nearby edges, with the required weights given explicitly by (33). Assuming that the grid geometry is completely given in terms of the lengths l_e and d_e and areas A_i, $A_v^{(\mathrm{v})}$, the scheme still allows some freedom in the choice of the weights $R_{i\,v}$ relating the cell divergence to the vertex divergence. This freedom may be used to optimize the overall accuracy of the scheme, for example.

When the scheme is extended to the case of variable f, some new freedom arises in exactly how the factors of f are handled: for example, velocity components may be multiplied by f before taking the weighted sum (8), after taking the weighted sum, or as some linear combination of these alternatives. The requirement for energy conservation, however, does constrain the options (Ringler et al., manuscript submitted to Journal of Computational Physics). The accuracy with which Rossby mode propagation is captured is sensitive to these details: the case of the longitude-latitude grid on the sphere is discussed by [25] and the case of a perfectly regular hexagonal grid on a β-plane

is discussed by [26].

In a companion paper (Ringler et al., manuscript submitted to Journal of Computational Physics) we discuss the extension of this scheme to the nonlinear case with variable f. We obtain a scheme that is energy conserving in the fully nonlinear case, and retains stationary geostrophic modes in the linear constant f limit.

Acknowledgment. This paper is Los Alamos report number LA-UR 09-03238.

References

[1] A. Arakawa, A., V.R. Lamb, Computational design of the basic dynamical processes of the UCLA general circulation model, in J. Chang (Ed), Methods in Computational Physics, vol 17, Academic Press, 1977, pp. 173-265.

[2] A. Arakawa, V.R. Lamb, A potential enstrophy and energy conserving scheme for the shallow-water equations, Mon. Weather Rev. 109 (1981) 18-36.

[3] J.M. Augenbaum, C.S. Peskin, On the construction of the Voronoi mesh on a sphere, J. Comput. Phys. 14 (1985) 177-192.

[4] L. Bonaventura, T. Ringler, Analysis of discrete shallow water models on geodesic delaunay grids with C-type staggering, Mon. Weather Rev. 133 (2005) 2351-2373.

[5] V. Casulli, R.A. Walters, An unstructured grid, three-dimensional model based on the shallow water equations, Int. J. Numer. Methods Fluids 32 (2000) 331-348.

[6] V. Casulli, P. Zanolli, Semi-implicit numerical modeling of nonhydrostatic free-surface flows for environmental problems, Math. Comp. Modelling 36 (2002) 1131-1149.

[7] M.J.P. Cullen, Integration of the primitive equations on a sphere using the finite element method, Quart. J. Roy. Meteorol. Soc. 100 (1974) 555-562.

[8] S. Dobricic, An improved calculation of Coriolis terms on the C grid, Mon. Weather Rev. 134 (2006) 3764-3773.

[9] M.S. Fox-Rabinovitz, Computational dispersion properties of 3D staggered grids for a nonhydrostatic anelastic system, Mon. Weather Rev. 124 (1996) 498-510.

[10] F.X. Giraldo, Lagrange-Galerkin methods on spherical geodesic grids: The shallow-water equations, J. Comput. Phys. 160 (2000) 336-368.

[11] R. Heikes, D.A. Randall, Numerical integration of the shallow-water equations on a twisted icosahedral grid. Part I: Basic design and results of tests, Mon. Weather Rev. 123 (1995) 1862-1887.

[12] A. Kageyama, T. Sato, "Yin-Yang grid": An overset grid in spherical geometry, Geochemistry Geophys. Geosystems 5 (2004) Art.No. Q09005.

[13] D. Majewski, D. Liermann, P. Prohl, B. Ritter, M. Buchhold, T. Hanisch, G. Paul, W. Wergen, The operational global icosahedral-hexagonal gridpoint model GME: Description and high-resolution tests, Mon. Weather Rev. 130 (2002) 319-338.

[14] Y. Masuda, H. Ohnishi, An integration scheme of the primitive equation model with an icosahedral-hexagonal grid system and its application to the shallow-water equations. In Short- and Medium-Range Numerical Weather Prediction. Collection of Papers Presented at the WMO/IUGG NWP Symposium, Tokyo, August 4-8, 1986. Japan Meteorological Society, 1986, pp. 317-326.

[15] H. Miura, M. Kimoto, A comparison of grid quality of optimized spherical hexagonal-pentagonal geodesic grids, Mon. Weather Rev. 133 (2005) 2817-2833.

[16] S. Ničković, M.B. Gavrilov, I.A. Tosić, Geostrophic adjustment on hexagonal grids, Mon. Weather Rev. 130 (2002) 668-683.

[17] M. Rančić, R.J. Purser, F. Mesinger, A global shallow-water model using an expanded spherical cube: Gnomonic versus conformal coordinates, Quart. J. Roy. Meteorol. Soc. 122 (1996) 959-982.

[18] D.A. Randall, Geostrophic adjustment and the finite-difference shallow-water equations, Mon. Weather Rev. 122 (1994) 1371-1377.

[19] T. Ringler, R. Heikes, R., D.A. Randall, Modeling the atmospheric general circulation using a spherical geodesic grid, Mon. Weather Rev. 128 (2000) 2471-2490.

[20] T. Ringler, D. Randall, A potential enstrophy and energy conserving numerical scheme for solution of the shallow-water equations on a spherical geodesic grid. Mon. Weather Rev. 130 (2002) 1397-1410.

[21] R. Sadourny, Numerical integration of the primitive equations on a spherical grid with hexagonal cells, in: Proceedings of WMO/IUGG NWP Symp., Tokyo, Japan, Japan Meteorological Agency, 1969, pp. 45-52.

[22] M. Satoh, T. Matsuno, H. Tomita, T. Nasuno, S. Iga, H. Miura, Nonhydrostatic Icosahedral Atmospheric Model (NICAM) for global cloud resolving simulations, J. Comput. Phys. 227 (2008) 3486-3514.

[23] G.R. Stuhne, W.R. Peltier, New icosahedral grid-point discretizations of the shallow water equations on the sphere, J. Comput. Phys. 148 (1999) 23-58.

[24] J. Thuburn, A PV-based shallow water model on a hexagonal-icosahedral grid, Mon. Weather Rev. 125 (1997) 2328-2347.

[25] J. Thuburn, Rossby wave propagation on the C-grid, Atmos. Sci. Lett. 8 (2007) 37-42.

[26] J. Thuburn, Numerical wave propagation on the hexagonal C-grid, J. Comput. Phys. 227 (2008) 5836-5858.

[27] J. Thuburn, A. Staniforth, Conservation and linear Rossby-mode dispersion on the spherical C grid, Mon. Weather Rev. 132 (2004) 641-653.

[28] D. Williamson, Integration of the barotropic vorticity equation on a spherical geodesic grid, Tellus 20 (1968) 624-653.